



HAL
open science

Green synthesis and characterization of $\text{Ni}_{0.8}\text{Zn}_{0.2}\text{Fe}_2\text{O}_4$ nano ferrite

Saurabh Raghuvanshi, Rulan Verma, Priyanka Tiwari, Frédéric Mazaleyrat,
Shashank Kane

► **To cite this version:**

Saurabh Raghuvanshi, Rulan Verma, Priyanka Tiwari, Frédéric Mazaleyrat, Shashank Kane. Green synthesis and characterization of $\text{Ni}_{0.8}\text{Zn}_{0.2}\text{Fe}_2\text{O}_4$ nano ferrite. *Advances in basic Science (ICABS 2019)*, Aug 2019, Bahal, India. pp.160002, 10.1063/1.5122583 . hal-04453089

HAL Id: hal-04453089

<https://hal.science/hal-04453089>

Submitted on 12 Feb 2024

HAL is a multi-disciplinary open access archive for the deposit and dissemination of scientific research documents, whether they are published or not. The documents may come from teaching and research institutions in France or abroad, or from public or private research centers.

L'archive ouverte pluridisciplinaire **HAL**, est destinée au dépôt et à la diffusion de documents scientifiques de niveau recherche, publiés ou non, émanant des établissements d'enseignement et de recherche français ou étrangers, des laboratoires publics ou privés.

Copyright

RESEARCH ARTICLE | AUGUST 29 2019

Green synthesis and characterization of $\text{Ni}_{0.8}\text{Zn}_{0.2}\text{Fe}_2\text{O}_4$ nano ferrite

S. Raghuvanshi; R. Verma; P. Tiwari; F. Mazaleyrat; S. N. Kane 



AIP Conf. Proc. 2142, 160002 (2019)

<https://doi.org/10.1063/1.5122583>



CrossMark



Cut Hall measurement time in *half* using an M91 FastHall™ controller



Also available as part of a tabletop system and an option for your PPMS® system

Green Synthesis And Characterization of $\text{Ni}_{0.8}\text{Zn}_{0.2}\text{Fe}_2\text{O}_4$ Nano Ferrite

S. Raghuvanshi¹, R. Verma¹, P. Tiwari^{1,2}, F. Mazaleyrat³ and S. N. Kane^{1, a)}

¹Magnetic Materials Laboratory, School of Physics, D. A. University, Indore-452001, India.

²Department of Physics, Prestige Institute of Engineering Management and Research, Indore-452010, India.

³SATIE, ENS Cachan, CNRS 8029, Universite Paris-Saclay, 61 Av. du Pdt. Wilson, F-94230, Cachan, France.

^{a)}Corresponding author: kane_sn@yahoo.com

Abstract. $\text{Ni}_{0.8}\text{Zn}_{0.2}\text{Fe}_2\text{O}_4$ nano-powders were prepared by solution combustion method by using metal nitrates, citric acid, green fuel (plant extracts). The structural, magnetic characteristics of as prepared, annealed $\text{Ni}_{0.8}\text{Zn}_{0.2}\text{Fe}_2\text{O}_4$ samples were determined by X-ray diffraction (XRD), Fourier Transform Infrared Spectroscopy (FTIR), vibrating sample magnetometer (VSM). XRD confirms the formation of single phase nano-crystalline (grain size: 12.7 – 32.7 nm) cubic spinel structure of annealed samples. Studied mixed ferrite shows relocation of Ni^{2+} , Zn^{2+} , Fe^{3+} ions between A, B site. Coercivity of annealed samples ranges between 29.7 to 124.9 Oe. Obtained saturation magnetization of annealed samples (34.56 – 54.96 Am^2/kg) is a combined effect of weakening of A-B, A-A, and strengthening of B-B interaction, and surface dead layer (0.80 – 1.25 nm) on particles, arising due to spin disorder at surface.

INTRODUCTION, SAMPLE SYNTHESIS, AND CHARACTERIZATION

Nano-crystalline spinel ferrites are magnetic ceramics of great implication in several nano-technological applications on account of their electrical, magnetic, dielectric properties [1]. In the last decade, a variety of chemical synthesis techniques (e. g. co-precipitation, electrochemical, hydrothermal, sol gel etc.) have been used to synthesize spinel ferrite nano-particles. At the present time, there is a great need to explore simple, environment friendly and cost effective techniques for production of spinel ferrite nano-particles. Recently, biosynthetic techniques utilizing either plant extracts or biological microorganisms have emerged as an easy and viable option to physical procedures, and chemical synthetic methods. Many researchers demonstrated the use of a simple synthetic process via economical precursors of honey, garlic, ginger, neem leaves, banana peel, cardamom seeds, and aloe vera plant extract, providing high yield nano- crystalline spinel ferrites with suitable magnetic properties [2]. Combination of bio-molecules e. g. - carbohydrates, flavonoids, phenols, polysaccharides, amino acids, terpenoids, etc. present in plant extracts are act as stabilizing, capping agents, and chelating agents [3]. In addition green synthesis is also helpful to reduce toxicity of nano-particles.

Among various spinel ferrites, zinc substituted nickel ferrites have attracted significant attention because of its easily tunable structural, magnetic properties, and sufficient biocompatibility [4]. Ni-Zn ferrites have gained substantial attention by the researchers because of their wide-ranging and excellent properties (e. g. - low magnetic coercivity, and high resistivity etc.). In the spinel structure of Ni-Zn, eight tetrahedral (A) sites taken by non-magnetic Zn^{2+} ions whereas sixteen octahedral (B) sites occupied by Fe^{3+} , Ni^{2+} ions. Owing to synthesis procedure, few irons on B site may be in the divalent (Fe^{2+}) state and influences the magnetic properties. In our previous work [5] we have studied dry gel $\text{Ni}_{0.8}\text{Zn}_{0.2}\text{Fe}_2\text{O}_4$ sample, which exhibits highest value of M_s (48.7 Am^2/kg) as well as good specific absorption rate, which is suitable for the hyperthermia applications. The structural and magnetic properties of spinel ferrites can be altered by substitution of nonmagnetic cations e. g. – Zn etc., different metal to fuel ratio or using various types of fuel. According to authors best knowledge no reports are available on comparative study of Ni-Zn ferrite synthesized by chemical fuel (e. g. - citric acid), and green fuel. The replacement of conventional fuel by another type of fuel is expected to produces various noticeable effects including changes in

cation distribution, structural, magnetic properties of $\text{Ni}_{0.8}\text{Zn}_{0.2}\text{Fe}_2\text{O}_4$ spinel ferrite system. Hence, it is interesting to investigate the structural, magnetic properties of $\text{Ni}_{0.8}\text{Zn}_{0.2}\text{Fe}_2\text{O}_4$ spinel ferrite prepared via sol gel auto combustion technique by using different type of plant extracts as fuel (chelating agent). In the present work, citric acid, and natural products (honey, garlic, ginger, aloe vera) were used for synthesizing $\text{Ni}_{0.8}\text{Zn}_{0.2}\text{Fe}_2\text{O}_4$ spinel ferrite. Further, effects of conventional fuel (citric acid), and green fuel (honey, garlic, ginger, aloe vera) on structural changes, cation distribution, and magnetic properties were investigated.

The metal nitrates ($1(\text{Ni}^{2+}, \text{Zn}^{2+}):2\text{Fe}^{3+}$) were added slowly under stirring to the honey/aloe vera gel/aqueous ginger root/aqueous garlic extract, respectively. Aqueous solution of ginger, and garlic was prepared as described elsewhere [3, 6]. The precursor mixtures (pH ~ 2) were heated at 110 °C in air till loose powder was formed, called as 'dry gel/as-burnt'. The self-combustion reaction is an exothermic redox process in which the mixture of nitrates and different plant extracts behave similarly to conventional oxidants, and fuels. $\text{Ni}_{0.8}\text{Zn}_{0.2}\text{Fe}_2\text{O}_4$ samples were synthesized by conventional and green fuel, for comparison between them. Prepared dry gel was annealed at 500 °C for 3 hrs to improve the degree of crystallization. Prepared as-burnt samples using various fuels were labelled: honey as S1, garlic as S2, ginger as S3, aloe vera as S4, whereas annealed samples were designated as follows: citric acid as S5, honey as S6, garlic as S7, ginger as S8, aloe vera as S9. Room temperature magnetic hysteresis loops of as-burnt, annealed samples were measured via vibration sample magnetometer 'VSM' (LakeShore Model 7410) with applied field of ± 1.8 Tesla, used to obtain saturation magnetization (M_s), coercivity (H_c). X-ray diffraction (XRD) patterns ($\theta - 2\theta$ geometry) of prepared dry gel, annealed samples were done by Bruker D8 diffractometer utilizing CuK_α radiation ($\lambda = 0.15406$ nm). Reitveld refinement software 'MAUD' (*Material Analysis Using Diffraction*) [7] was used for full proof analysis of XRD patterns to obtain experimental lattice parameter (a_{exp}). Cation distribution was determined by using XRD data, employing Bertaut method, as explained in [8]. Theoretical lattice parameter (a_{th}), theoretical/Néel magnetic moment ($M_{s(t)}$), bond angles ($\theta_1 - \theta_3$), were obtained by cation distribution [9]. Fourier Transform Infrared Spectra (in absorption mode) were obtained by Perkin-Elmer FTIR spectrometer. Bulk saturation magnetization ($M_{s(B)}$), dead layer thickness (t) were obtained as described in [10].

RESULTS AND DISCUSSION

The x-ray diffraction (XRD) patterns of as-burnt, and annealed $\text{Ni}_{0.8}\text{Zn}_{0.2}\text{Fe}_2\text{O}_4$ (S1 – S9) spinel ferrite powders are presented in Fig. 1a (inset i, ii also shows magnetic data) and 1b respectively. Representative Rietveld refined XRD plot for selected $\text{Ni}_{0.8}\text{Zn}_{0.2}\text{Fe}_2\text{O}_4$ composition (S6) of annealed samples illustrated in Fig. 1 (c). XRD peaks for as-burnt S1 sample confirms the formation of single phase cubic spinel structure, but other samples are not showing formation of spinel phase. Observed behaviour of sample S1 is ascribed honey serves the role of a better chelating agent as compared to other plant extracts. All annealed (500 °C for 3hrs.) $\text{Ni}_{0.8}\text{Zn}_{0.2}\text{Fe}_2\text{O}_4$ samples confirm the formation of single phase (no secondary phase) nanocrystalline cubic spinel structure (space group Fd3m), ascribed as role of thermal annealing facilitates formation of spinel phase. The structural parameters: experimental, theoretical lattice parameter (a_{exp} , a_{th}), Scherrer's grain size (D), x-ray density (ρ_{XRD}), specific surface area (S) and cation distribution for sites A, B of annealed samples obtained by analyzing XRD data, are illustrated in table 1. Observed changes in a_{exp} , a_{th} of the studied samples can be attributed to the role of different fuel used for synthesis, helps in relocating the ions having dissimilar ionic radii (*ionic radius of Ni^{2+} : 0.069 nm, and Zn^{2+} : 0.074 nm*), which changes microstructure of samples (*reflected in ρ_{XRD} , a_{exp} etc.*). Grain size of annealed samples range between 12.7–32.7 nm, where D for sample S1 (which is dry gel) is 23.5 nm, clearly shows formation of nano-crystalline spinel ferrite. D of annealed S6 sample increases (24.9 nm) as compared to S1 sample (as-burnt) is attributed to effect of annealing responsible for grain growth in the sample. Variation in D of the studied annealed samples with citric acid and different plant extracts is attributed to the effect of reaction condition, which favors the formation of new nuclei preventing further growth of particles. Ferrites play a crucial role in improving the solid catalysts performance due to their superior surface to bulk ratio. There is an opposite relationship between D and ρ_{XRD} with S [10]: smaller the grain size, larger is the surface area. Specific surface area of the studied annealed samples varies from 34.3 – 88.5 m^2/g . For sample S9, obtained high S (88.5 m^2/g) value makes it more suitable for catalytic activity.

Cation distribution was obtained by XRD analysis, depicted in table 1 for annealed $\text{Ni}_{0.8}\text{Zn}_{0.2}\text{Fe}_2\text{O}_4$ samples. It is worth noting that, Zn ferrite shows normal spinel structure, whereas Ni ferrite displays inverse spinel structure. However, the sample reported in present study contains both Zn^{2+} and Ni^{2+} , would reveal mixed ferrite with presence of both Ni^{2+} and Zn^{2+} on both A and B sites. The presence of Ni^{2+} , Zn^{2+} and Fe^{3+} ions on A, B site (see table 1) clearly shows the mixed ferrite structure as expected. Observed close matching of a_{exp} , and a_{th} suggest that the calculated distribution of cations among A, B sites is in good agreement with the actual distribution. In our samples,

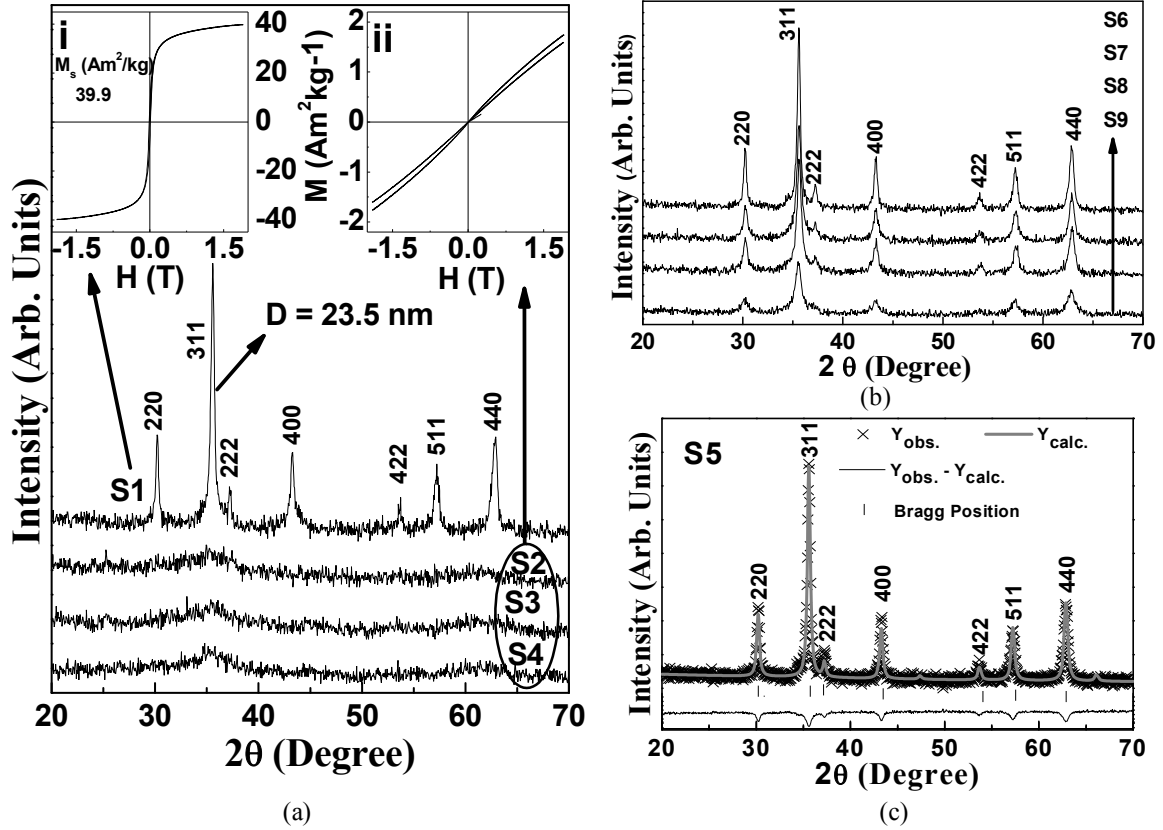


FIGURE 1. XRD patterns of (a) as-burnt Ni-Zn ferrite obtained by using honey *S1*, garlic *S2*, ginger *S3*, aloe vera *S4*, Inset: Hysteresis loop of as-burnt (i) *S1* (ii) *S2*, *S3*, *S4*. (b) XRD patterns of *S6*–*S9* samples. (c) Rietveld refined XRD of *S5* sample

the non magnetic Zn^{2+} ions (zero magnetic moment) are distributed at both A, B sites whereas large fraction of magnetic Ni^{2+} ions (magnetic moment = $2 \mu_B$) reside on B site. Observed changes in cationic distribution clearly show its strong dependence on the used fuel (citric acid and green fuel).

The IR spectra of annealed samples are shown in Fig. 2 and band positions are presented in table 2. There are two absorption bands in the ranges $200 - 650 \text{ cm}^{-1}$ which are characteristic of two Me–O absorption bands for spinel ferrites. The first one between $570 - 590 \text{ cm}^{-1}$ corresponds to vibrations of the tetrahedral cations $Me_A\text{-O}$, and the second one between $397 - 398 \text{ cm}^{-1}$ corresponds to vibrations of the octahedral cations $Me_B\text{-O}$. Observed shift in band positions for studied annealed samples is caused by variation of ionic distances $Fe_B\text{-O}$, and $Fe_A\text{-O}$. Absorption bands provide information on the formation of cubic spinel structure, which is in agreement with XRD results. In order to estimate the strength of bonding between $Fe^{3+} - O^{2-}$ ions the force constants for tetrahedral (A) and octahedral (B) sites (K_T , K_O) were calculated using the relation: $K = 4\pi^2 c^2 \nu^2 \mu$, where ν is high-frequency or low-frequency band, c is velocity of light ($c = 2.99 \times 10^8 \text{ m/s}$), and μ is reduced mass of the vibrating atoms. Obtained values of the K_T and K_O are listed in table 2. It is worth mentioning that the force constants are inversely proportional

TABLE 1. Experimental, theoretical lattice parameter (a_{exp} , a_{th}), grain diameter (D), x-ray density (ρ_{XRD}), specific surface area (S) and distribution of cations between A, B site of annealed Ni-Zn samples.

Sample	a_{exp} (nm)	a_{th} (nm)	D (nm)	ρ_{XRD} (kg/m ³)	S (m ² /g)	Cation distribution	
						A - site	B - site
S5	0.8363	0.8360	32.7	5354.0	34.3	$(Ni^{2+}_{0.00}Zn^{2+}_{0.18}Fe^{3+}_{0.82})$	$[Ni^{2+}_{0.80}Zn^{2+}_{0.02}Fe^{3+}_{1.18}]$
S6	0.8359	0.8361	24.9	5360.9	44.9	$(Ni^{2+}_{0.00}Zn^{2+}_{0.20}Fe^{3+}_{0.80})$	$[Ni^{2+}_{0.80}Zn^{2+}_{0.00}Fe^{3+}_{1.20}]$
S7	0.8355	0.8358	17.3	5368.8	64.6	$(Ni^{2+}_{0.05}Zn^{2+}_{0.10}Fe^{3+}_{0.85})$	$[Ni^{2+}_{0.75}Zn^{2+}_{0.10}Fe^{3+}_{1.15}]$
S8	0.8351	0.8358	17.6	5376.7	63.4	$(Ni^{2+}_{0.04}Zn^{2+}_{0.10}Fe^{3+}_{0.86})$	$[Ni^{2+}_{0.76}Zn^{2+}_{0.10}Fe^{3+}_{1.14}]$
S9	0.8369	0.8357	12.7	5340.9	88.5	$(Ni^{2+}_{0.07}Zn^{2+}_{0.05}Fe^{3+}_{0.88})$	$[Ni^{2+}_{0.73}Zn^{2+}_{0.15}Fe^{3+}_{1.12}]$

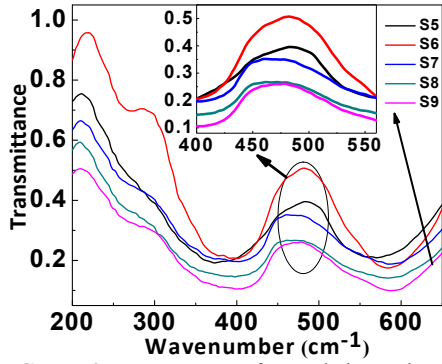


FIGURE 2. FTIR spectra of annealed samples.

TABLE 2. IR absorption tetrahedral, octahedral bands (ν_1 , ν_2), force constants (K_T , and K_O) and Debye temperature (θ_D) of annealed $\text{Ni}_{0.8}\text{Zn}_{0.2}\text{Fe}_2\text{O}_4$ system.

Sample	ν_1 (cm ⁻¹)	ν_2 (cm ⁻¹)	$K_T \times 10^5$ (dyne/cm ²)	$K_O \times 10^5$ (dyne/cm ²)	θ_D (K)
S5	570.97	374.05	2.3759	1.0197	678.47
S6	584.42	401.24	2.4892	1.1733	707.64
S7	584.35	402.83	2.4886	1.1826	708.73
S8	584.32	397.05	2.4883	1.1489	704.80
S9	586.17	399.33	2.5041	1.1622	707.53

to the bond lengths between oxygen ions and metallic cations in the corresponding positions of spinel crystal lattice [11]. The Debye temperature (θ_D) for annealed samples was calculated as given in [11], and values of θ_D are described in table 2. Observed variation in θ_D is associated to the changes in wave number of the peak usually credited to Me-O bond vibration in the tetrahedral (A) sites. Obtained higher value of θ_D (table 2) for sample S7, implies presence of garlic extract supporting the enhancement of the lattice vibrations.

It is worth noting that the magnetization of the ferrite system is directly proportional to the exchange interaction between A, B sub-lattices. Bond angles among A-O-B (θ_1 , θ_2), B-O-B site (θ_3 , θ_4) and A-O-A site (θ_5) provide information on magnetic interaction between cations on A and B sites. Variation of bond angles in the studied samples is described in table 3. Obtained lowest value of bond angles θ_1 , θ_2 , θ_5 and highest value of bond angles θ_3 , θ_4 for S6 compared to the other samples implies weakening of A-B, A-A, strengthening of B-B interaction.

Movement of O²⁻ ion (oxygen parameter u) due to the rearrangement of cations at A site reflects alteration in spinel structure. Observed value of u parameter of the studied samples range between 0.3797-0.3807, which are greater than the ideal value ($u_{ideal} = 0.375$) of the spinel ferrites [9] reveals distortion in the spinel structure. Figure 3a depicts the hysteresis loop of the studied annealed samples, whereas inset 3a(i) displays coercivity (H_c) variation with D, and inset 3a(ii) depicts variation of M_s (at 300 K) with S . Coercivity values of annealed samples range between 29.7 – 124.9 Oe. Perusal of inset (i) of Fig. 3a shows that H_c increases with the grain size, suggests studied system lies in the overlap between single-multi domain regions. Bulk magnetization has value of 68.17 Am²/kg, obtained by plotting M_s vs S , and extrapolating the data to $S = 0$ (Inset ii of Fig. 3a). Figure 3b depicts variation of experimental M_s (at 300 K), and theoretical $M_{s(t)}$ (at 0 K) of annealed samples. Highest M_s of 54.96 Am²/kg was obtained for the annealed S6 sample as compared to other annealed samples, while as-burnt S1 sample provides value of M_s is 39.88 Am²/kg. Obtained M_s (300 K) values were lower than $M_{s(t)}$ (shown in inset ii of Fig. 3a) value clearly shows the presence of surface dead layer t (table 4) on particles, arising due to spin disorder at surface [10]. It should be noted that with citric acid, and various plant extracts the obtained $M_{s(t)}$ values is a consequence of different fraction of Ni²⁺ and Zn²⁺ ions on A and B sites (table 1). Perusal Fig. 3b shows linear variation of M_s , inversion parameter δ with u , while inset demonstrates linear variation of M_s with δ . Obtained variation clearly confirms that both u , δ contribute decisively in tuning M_s of the studied samples. It is worth noting that increase of M_s with u or δ is ascribed to higher distortion in the spinel structure, expected to affect the magnetization. Perusal of Fig. 3b also depicts that as degree of inversion ' δ ' (determining by unusual occupancy of the ions on A, B site) increases results in increasing distortion (u) in the spinel structure which is very clearly reflected by observed changes in M_s , displays the importance of cationic distribution (on A, B site) in determining magnetic properties.

TABLE 3. Variation of bond angles (θ_1 , θ_2 , θ_3 , θ_4 , θ_5) of annealed $\text{Ni}_{0.8}\text{Zn}_{0.2}\text{Fe}_2\text{O}_4$ system.

Sample	θ_1 (°) (A-O-B)	θ_2 (°) (A-O-B)	θ_3 (°) (B-O-B)	θ_4 (°) (B-O-B)	θ_5 (°) (A-O-A)
S5	123.51	145.73	92.59	125.86	74.95
S6	123.44	145.42	92.69	125.88	74.77
S7	123.60	146.13	92.45	125.83	75.19
S8	123.59	146.10	92.46	125.83	75.18
S9	123.76	146.89	92.20	125.80	75.65

TABLE 4. Dead layer thickness (t), experimental, theoretical magnetization (M_s , $M_{s(t)}$).

Sample	t (nm)	M_s (Am ² /kg)	$M_{s(t)}$ (Am ² /kg)
S5	1.25	52.58	80.55
S6	0.80	54.96	85.29
S7	0.99	44.81	68.70
S8	1.01	44.75	67.28
S9	1.04	34.56	59.70

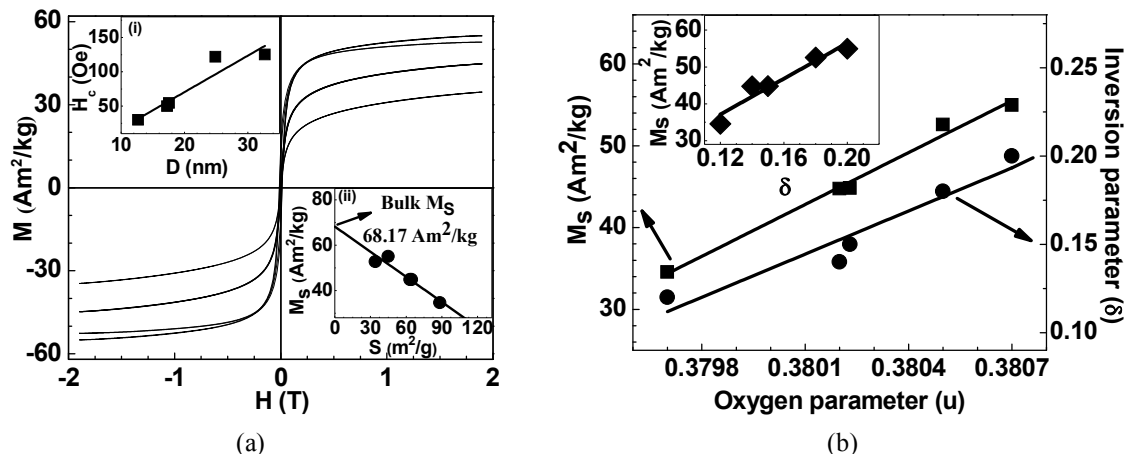


FIGURE 3. (a) Hysteresis loops of the annealed samples. Inset(s): (i) Variation of H_c with D . (ii) Specific surface area S dependence of saturation magnetization M_s . (b) Variation of experimental saturation magnetization M_s and inversion parameter δ with oxygen parameter u . Inset: Variation of M_s with δ . Continuous lines are linear fit to the experimental data

CONCLUSION

To summarize, the synthesis of nano-sized ferrite using natural product avoids the usage of harmful and toxic reducing agent in combustion method, would result in reduced toxicity. The use of natural products is a simple, environment friendly and well-organized route for formation of $\text{Ni}_{0.8}\text{Zn}_{0.2}\text{Fe}_2\text{O}_4$ ferrite. The X-ray diffraction study revealed the cubic structural phase formation of only S1 sample, and for all the annealed Ni-Zn spinel nanoferrite. The significant influence of citric acid, and various plants extract on the grain size, structural changes, and magnetic properties of Ni-Zn ferrite nano-particles are observed. Observed correlation between magnetic, and structural parameters was found due to cation distribution, and crystallite size effect. The observed maximum M_s value for S6 sample is ascribed to the major elements of honey (glucose, fructose) acting as a chelating agent on the development of nano-particles as viscous medium, natural reductant, and protecting agent as compared to other conventional fuel (citric acid), and green fuel(s) (plants extract).

ACKNOWLEDGEMENT

Work, SR are funded by Project: CSR-IC/CRS-74/2014-15/2104. Authors thank Dr. M. Gupta, Dr. U. P. Deshpande, UGC-DAE CSR, Indore for XRD, FTIR measurements. SNK thanks for a one month invited professor stay during Nov-Dec 2017 at ENS Paris-Saclay, Cachan, France.

REFERENCES

1. S. Raghuvanshi, F. Mazaleyrat and S. N. Kane, *AIP Advances* **8**, 047804-1–11 (2018).
2. R. S. Yadav, I. Kuřitka, J. Vilcakova, J. Havlica, J. Masilko, L. Kalina, J. Tkacz, J. Švec, V. Enev and M. Hajdúchová, *Adv. Nat. Sci: Nanosci. Nanotechnol.* **8**, 045002-1–14 (2017).
3. D. Gingasu, L. Mindru, S. Preda, J. M. Calderonmoreno, D. C. Culita, L. Patron and L. Diamandescu, *Rev. Roum. Chim.*, **62**, 645–653 (2017).
4. M. S. Al-Qubaisi, A. Rasedee, M. H. Flaifel, S. H. J. Ahmad, S. Hussein-Al-Ali, M. Z. Hussein, E. E. M. Eid, Z. Zainal, M. Saeed, M. Ilowefah, S. Fakurazi, N. M. Isa and M. E. E. Zowalaty, *Int. J. Nanomedicine* **8**, 2497–2508 (2013).
5. M. Coisson, G. Barrera, F. Celegato, L. Martino, S. N. Kane, S. Raghuvanshi, F. Vinai and P. Tiberto, *Biochimica et Biophysica Acta*, **1861**, 1545–1558 (2017).
6. G. VonWhiteII, P. Kerscher, R. M. Brown, J. D. Morella, W. McAllister, D. Dean and C. L. Kitchens, *J. Nanomaterials*, **2012**, 730746-1–12 (2012).
7. L. Lutterotti, and P. Scardi, *J. Appl. Cryst.*, **23**, 246–252 (1990).

8. L. Gastaldi, and A. Lapicciarella, [J. Sol. Stat. Cham.](#), **30**, 223–229 (1979).
9. J. Smit, H. P. J. Wijn, *Ferites* (Philips Technical Library, Eindhoven, 1959).
10. Z. X. Tang, C. M. Sorensen, K. J. Klabunde, and G. C. Hadjipanayis, [Phy. Rev. Letters](#), **67**, 3602–3605 (1991).
11. S. N. Kane, S. Raghuvanshi, M. Satalkar, V. R. Reddy, U. P. Deshpande, T. R. Tatarchuk and F. Mazaleyrat, *AIP Conf. Proc.*, **1953**, 030089–1–4 (2018).